Langmuir

ARTICLE

pubs.acs.org/Langmuir

Nanoparticle Flotation Collectors: Mechanisms Behind a New Technology

Songtao Yang, Robert Pelton,* Adam Raegen, Miles Montgomery, and Kari Dalnoki-Veress

McMaster University, 1280 Main Street West, Hamilton, Ontario, Canada L8S 4L7

ABSTRACT: This is the first report describing a new technology where hydrophobic nanoparticles adsorb onto much larger, hydrophilic mineral particle surfaces to facilitate attachment to air bubbles in flotation. The adsorption of 46 nm cationic polystyrene nanoparticles onto 43 μm diameter glass beads, a mineral model, facilitates virtually complete removal of the beads by flotation. As little as 5% coverage of the bead surfaces with nanoparticles promotes high flotation efficiencies. The maximum force required to pull a glass bead from an air bubble interface into the aqueous phase was measured by micromechanics. The pull-off force was 1.9 μN for glass beads coated with nanoparticles, compared to 0.0086 μN for clean beads. The pull-off forces were modeled using Scheludko's classical expression. We propose that the bubble/bead contact area may not be dry (completely dewetted). Instead, for hydrophobic nanoparticles sitting on a hydrophilic surface, it is possible that only the nanoparticles penetrate the air/water interface to form a three-phase contact line. We present a new model for pull-off forces for such a wet contact patch between the bead and the air bubble. Contact angle measurements of both nanoparticle coated glass and smooth films from dissolved nanoparticles were performed to support the modeling.

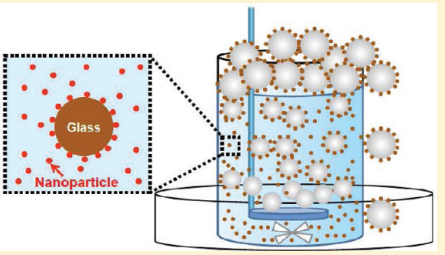

INTRODUCTION

Annually around 400 million metric tons of mineral is crushed and ground to particles, typically less than 100 μm in diameter, and then subjected to a process called froth flotation to isolate the valuable components.[1] A critical aspect in flotation is the use of low molecular weight, water-soluble amphiphilic molecules called collectors. Ideally, the collectors selectively bind to those particles rich in the desired mineral, rendering their surfaces more hydrophobic than the undesirable gangue particles. In the flotation process, the more hydrophobic mineral particles attach to air bubbles, rising through the suspension, and the desired mineral particles are carried away with the foam froth. Conventional collectors are low molecular weight surfactants with head groups such as xanthate that promote adsorption on the mineral surfaces. This paper is the first report of a completely new class of collectors based on hydrophobic nanoparticles.

A typical conventional collector is potassium amyl xanthate with an extended molecular length of about 1 nm. By contrast, the work herein involves nanoparticle collectors based on polystyrene with diameters varying between 46 and 120 nm. We report both laboratory scale flotation experiments with glass spheres, a model for mineral particles, and micromechanics[2,3] experiments measuring the force required to detach nanoparticle-coated glass spheres from air bubbles. The goal of our work was to develop an understanding of the mechanisms by which nanoparticles promote flotation with a view to predicting the role of nanoparticle diameter and hydrophobicity on flotation. The following paragraphs briefly summarize the relevant literature, giving some context for our work.

A recent publication edited by Fuerstenau, Jameson, and Yoon[1] gives a good summary of the current understanding of flotation mechanisms. A typical approach to flotation modeling is to divide flotation into a sequence of steps and to develop a probability expression for each step. Nanoparticle flotation collectors are likely to influence two important steps in the sequence of flotation mechanisms: the attachment of the mineral particle to the air bubble surface after collision, and the unwanted detachment of the mineral particles from the bubbles. Ralston et al. argue that the attachment step involves three processes: (1) thinning of the intervening liquid film between the mineral particle and the bubble; (2) rupture of the film to give a three-phase contact "nucleus"; and (3) expansion of the three-phase contact line from the nucleus to form a stable wetting perimeter.[4] The impact of adsorbed nanoparticles on mineral particle/bubble attachment will be addressed in the Discussion section.

The importance of the water contact angle on the mineral surface has been emphasized since the earliest flotation studies.[5] Ralston's group has published detailed flotation kinetic models accounting for hydrodynamic and capillary forces, and model predictions gave good agreement with experimental data.[6,7] A more pessimistic view is given by Chau et al. in their recent review: "So far, there is no rigid quantitative correlation of contact angle on flotation rate recovery."[8] Contact angle hysteresis and pinning of the three-phase contact line complicate modeling.[9−12] Herein we employ polystyrene nanoparticle collectors that we will show increase the contact angle of hydrophilic glass surfaces. Ordered monolayers of monodisperse tridecafluorooctyltriethoxysilane modified polystyrene particles give very high water contact angles[13] even when the particle surfaces are etched to give large distances between the particles.[14] Similarly, a number of studies has

Received: May 4, 2011
Revised: July 20, 2011
Published: July 26, 2011

dx.doi.org/10.1021/la2016534 | *Langmuir* 2011, 27, 10438–10446

shown that randomly deposited latex can give high contact angles.[13−16]

Fetzer and Ralston recently reported bubble-surface attachment studies[17] and found that the overall dewetting−attachment step occurs in less than a millisecond. The initial dewetting is very rapid with a low contact angle; they argue that a hydrodynamic model fits this behavior. At longer times, the dewetting rate is lower and the corresponding contact angle is higher. This behavior was explained by pinning on hydrophilic patches. The surfaces used in that study were chemically heterogeneous but topologically smooth. Herein we present contact angle measurements for hydrophilic glass surfaces decorated with hydrophobic polystyrene nanoparticles; the maximum force required to dislodge 43 μm glass spheres from air bubbles; and glass sphere flotation in the presence of nanoparticle flotation collectors.

EXPERIMENTAL SECTION

Materials. Styrene (99%, Sigma-Aldrich) was purified by vacuum distillation. 3-(Methacryloylamino)propyl trimethyl ammonium chloride solution (MAPTAC, 50 wt % in H_2O, Sigma-Aldrich) was passed through inhibitor-removing columns. Cetyltrimethylammonium bromide (CTAB, 95%) and 2,2′-azobis(2-methylpropionamidine) dihydrochloride (V50, 97%) were purchased from Sigma-Aldrich and used as supplied. UNIFROTH 250C (99%), a mixture of monomethyl polypropylene glycol, 250 kDa and dipropylene glycol monomethyl ether, was donated by VALE Canada (Mississauga, ON) and was used as supplied. All solutions were made with Type 1 water (Barnstead Nanopure Diamond system).

Polymerizations. The polystyrene-*co*-MAPTAC (St-MAPTAC-02-120) latex was prepared by batch emulsion polymerization,[18] whereas St-01-46 was prepared by monomer-starved semibatch emulsion polymerization.[19] The polymerizations were conducted in a three-necked flask equipped with a condenser, two rubber stoppers holding syringe needles (one for nitrogen, the other for monomer addition if the starved-feed charge was employed), and a magnetic stirring bar (controlled by a IKAMAG RCT basic hot plate/stirrer, NC). For St-MAPTAC-02-120, 100 mL of deionized water was charged to the reactor, followed by nitrogen purging for 30 min at 70 °C with 350 rpm stirring. To the reactor were added 5.0 g of styrene and 0.25 g of 50 wt % MAPTAC. After 10 min equilibration, 0.1 g of V50 initiator, dissolved in 10 mL of water, was injected to initiate the polymerization.

For St-01-46, after 15 min polymerization of the initial charge of 0.5 g of styrene, in 100 mL of water with 0.10 g of CTAB and 0.1 g of V50, an additional 4.5 g of styrene was added over 5 h (0.0083 mL/min) from a 10 mL syringe fitted to a syringe pump (NE-1600, New Era Pump System, Inc.). The reaction was stirred at 70 °C for an additional 19 h. The resulting latex was dialyzed for at least 5 days against deionized water, after which the dialysate conductivity was less than 20 μS/cm.

Nanoparticle hydrodynamic diameters were determined by dynamic light scattering (Brookhaven Instruments Corporation, BIC) using a detector angle of 90°. Correlation data were analyzed by BIC dynamic light scattering software (Windows 9KDLSW version 3.34) using the cumulant model, whereas the CONTIN model was used to generate the particle size distributions. The scattering intensity was set between 150 and 250 kcounts/s for each measurement. The duration for each measurement was set to 5 min. Electrophoretic mobility (EM) measurements were performed by using a Zeta PALS instrument (Brookhaven Instruments Corp.) at 25 °C in phase analysis light scattering mode. The reported EM values were the average of 10 runs, with each consisting of 15 scans. Samples for both dynamic light scattering and electrophoretic mobility measurements were prepared in clean vials by dispersing approximately 0.25 g/L of polystyrene nanoparticles in 5 mM NaCl.

Contact Angle Measurements. Water contact angle measurements were performed on glass microscope slides (Gold Line Microscope Slides, VWR), which we assumed had similar surface characteristics as the glass beads. In a typical experiment, glass microscope slides were cut to approximated 9.5 mm squares, cleaned (Sparkleen detergent, Fisher Scientific), and immersed in 300 mg/L (for St-01-46) nanoparticle suspension in 5 mM NaCl for times ranging from 10 to 30 min. The treated slides were immersed in ∼1000 mL of water to remove unbound nanoparticles.

The water/air contact angle with treated slides was determined either by using conventional sessile drops placed on dry slides or by observing air bubbles attached to never-dried latex treated glass slides immersed in water. For the latter measurements, air bubbles were formed on thin glass capillary tubes. Standard glass capillaries (1 mm/0.58 mm OD/ID, Word Precision Instruments INC., 1B100-6) were elongated using a pipet puller (Narishige Japan, PN-30). An electrical transformer supplied 2 V to to heat a Pt:Ir (90:10 wt %, diameter 0.5 mm) wire, and the pipet was bent around the wire at a position approximately 5−6 mm from the chokepoint after pulling. The metal wire was then quickly cooled by turning off the transformer, causing the capillary to break cleanly, yielding a capillary with an outer diameter of 20−40 μm.

Air bubbles were formed on the capillary and slowly pushed in contact with treated glass slides, transferring the bubble to the surface. The contact angle measurements were performed using a Krüss contact angle measuring instrument running Drop Shape Analysis (DSA) 1.80.0.2 software. Advancing and receding angles were generated by carefully pushing or pulling the bubble with the glass capillary.

In order to access the hydrophobicity of the nanoparticle surfaces, samples were dried and dissolved in THF (tetrahydrofuran (Certified), Fisher Scientific), 0.65 wt %, and spin coated (SPIN 150 Wafer Spinner running rev: 3.25 software) on glass at 3000 rpm.

Glass Beads. Glass beads (30−50 μm) were purchased from Polysciences Inc. The particle size distributions of the glass beads in 5×10^{-3} M NaCl were measured with a Malvern Mastersizer 2000 instrument. The particle size distributions were approximately log-normal with an area averaged mean diameter of 43 μm, a standard deviation of 11 μm, and a corresponding specific surface area of 0.057 m^2/g. The electrophoretic mobility of the beads in in 5 mM NaCl at ambient pH was $-4.61\ (\pm 0.32) \times 10^{-8}\ m^2\ s^{-1}\ V^{-1}$.

Flotation. In a typical flotation experiment, 2 g of glass beads and 1.0 mL of nanoparticles (14.6 g/L for St-MAPTAC-02-120) were added into 120 mL of 5×10^{-3} M NaCl in a 150 mL plastic flotation beaker, sitting on a 90 mm diameter plastic Petri dish, which in turn was sitting on a magnetic stirrer (Corning Stirrer, model PC-160). The suspension of glass beads and polystyrene nanoparticles was mixed for 5 min (25 mm × 25 mm cross-shape stirring bar at ∼600 rpm) to facilitate polystyrene nanoparticle deposition onto the glass beads. Next 0.12 mL of 1% UNIFROTH 250C (10 ppm) was added and mixed for an additional 30 s. Flotation was commenced by initiating nitrogen flow (Matheson 604 E700 Flow Controller) at a rate of 2.0 L/min through a Corning Pyrex gas dispersion tube (Fisher Scientific, 11-137E) consisting of a 30 mm coarse glass frit attached by a 90° elbow. During flotation, the stirring rate was increased to ∼900 rpm to avoid bead sedimentation. The foam phase was scraped over the edge of the beaker and collected in the plastic Petri dish. After 1.0−1.5 min, the gas flow was stopped and the plastic collection dish was replaced with a clean dish. The liquid level in the flotation beaker was then topped up with UNIFROTH 250C in 5 mM NaCl at the original concentration. In most of our flotation cases, this sequence was repeated until three to five dishes were collected.

The mass of liquid and beads collected in each dish was measured; the beads were filtered with a Büchner funnel, dried, and weighed. Typically each dish contained 50−60 mL of flotation liquor. The flotation results were expressed as the recovery, the mass fraction of beads which were recovered in the dishes.

Table 1. Some Properties of the Polystyrene-Based Nanoparticle Collectors

nanoparticle designation	diameter, nm (PDI)[a]	electrophoretic mobility × 10^{-8} m^2 s^{-1} V^{-1} (std error)	contact angle smooth polymer film, θ_{np}[b]	contact angle of bubbles on glass, θ (std error)[b]
St-01-46	46 (0.156)	1.61 (±0.07)	91 (+0.9)	40 (±1.6)
St-MAPTAC-02-120	120 (0.027)	2.74 (±0.12)	85 (±1.7)	23 (±1.2)

[a] Hydrodynamic diameter from DLS using cumulant model. [b] Static contact angles of submerged bubbles; for examples, see Figure 5.

The extent of nanoparticle deposition on the glass beads was determined by measuring the absorbance of the supernatant nanoparticle dispersion at 500 nm (Beckman Coulter, DU800) before and after deposition (usually 7 min) on the glass beads. The quantity of deposited latex was calculated using a calibration curve of absorbance versus nanoparticle concentration.

Images of recovered glass beads from nanoparticle flotation runs were acquired by using a JEOL JSM-7000F scanning electron microscope.

Micromechanics. The adhesion experiment that we employed is similar to that of Colbert et al.,[3] with some alterations. In our experiment, a glass capillary was pulled to a very thin (~20 μm diameter), long, hollow pipet. This pipet was then bent into a "Z"-shape using right angles, with the first bend roughly 2 mm from the end and the second bend roughly 1.5 cm from the first, very near the thick, undeformed capillary. This shape allows for the deflection of the pipet to be directly calibrated and used as a force transducer in experiments.

A chamber containing many micrometer-sized particles was placed on a microscope positioned between two three-axis stages (Newport 462 XYZ) one of which was atop an additional linear stage (Newport VP-25XA). Using optical table mounts and 1″ posts, we mounted the pipet such that the thin, bent parts could move freely within the chamber. Using a syringe and Tygon tubing, suction was used to pick up a bead with the pipet. Using the second (motorized) stage and similar parts, the end of a capillary tube was placed in the chamber while nearly full of liquid, creating a small bubble in the tube. A syringe and tubing were likewise used to move the air until a portion of it was extended beyond the capillary. Pressure could then be exerted on the tubing in order to finely control the size of the free portion of the bubble (its radius of curvature). After aligning the center of the bubble and bead, the motor was moved until contact was made and then used to pull the bubble and bead apart, meanwhile monitoring the bubble shape and pipet deflection.

Pipets were calibrated by holding them vertically and imaging them from the side. As water was slowly pushed out of the end, the drop adhered to the end of the pipet in the unduloidal shape typical of a drop on a fiber, exerting a downward gravitational force. By fitting the shape of the drop and measuring the vertical displacement of the end of the pipet, we were able to find the force constant of each pipet, ranging from 0.005 to 0.1 μN/μm. Graphs of gravitational force versus pipet displacement were remarkably linear over the range in which they were used (up to displacements on the order of tens of micrometers), allowing for simple Hookian spring constants to be obtained. The spring constant multiplied by the bead displacement under load gave the force on the particle and pipet.

RESULTS

Two polystyrene copolymer nanoparticle dispersions were prepared by emulsion copolymerization. The resulting dispersions were colloidally stabilized by cationic amidine moieties[18] from the initiator and by quaternary ammonium surface groups from the MAPTAC monomer. Particle size distributions of the nanoparticles were measured by dynamic light scattering, and the results are summarized in Table 1 together with the electrophoretic mobilities. Both nanoparticle dispersions were cationic, with St-MAPTAC-02-120 having the greater electrophoretic mobility.

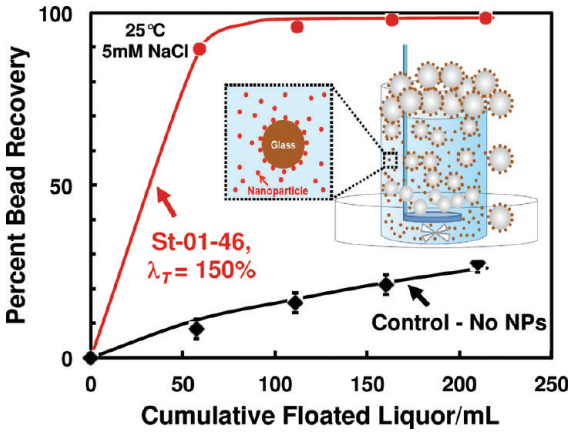

Figure 1. Glass bead flotation with and without St-01-46 nanoparticles. The *Y*-axis gives the fraction of added beads collected in the froth. Each point represents the contents of a froth collection dish.

Small scale, batch laboratory flotation experiments were conducted to demonstrate the ability of the nanoparticles to function as flotation collectors. Glass beads with a mean diameter of 43 μm were employed as model mineral particles. A total of 2 g of glass beads was suspended in 0.01 g/L frother, a nonionic surfactant, dissolved in 5 mM NaCl at pH 6.7. Figure 1 compares flotation results with and without the presence of nanoparticle flotation collector St-01-46, a 46 nm cationic polystyrene nanoparticle. The *X*-axis gives the volume of liquid from froth collected in 4 dishes during a flotation experiment. The *Y*-axis gives the cumulative mass fraction of added beads collected in the froth. Without nanoparticle collectors, the fraction of recovered beads increased linearly up to a maximum of about 30%. This was due to hydraulic entrainment, where beads suspended in the water phase were carried over with the water; this is a general effect in flotation.[1] With nanoparticles, virtually all of the beads were removed with the froth after the first couple of dishes (points). Herein we express the nanoparticle concentration in the flotation experiments as a theoretical coverage, λ_T, defined as the total projected area of the added nanoparticles divided by the total area of the glass beads. Then for the results in Figure 1, λ_T was 150%, meaning there were sufficient nanoparticles to form a saturated adsorbed layer on the glass beads. Note that the cationic nanoparticles spontaneously adsorbed onto the negatively charged beads. We will now consider what coverage or extent of nanoparticle adsorption was necessary to promote bead attachment to air bubbles and removal with the froth.

A series of flotation experiments was conducted in which the nanoparticles were first deposited on the beads, then the nondeposited nanoparticles were removed after 5 min, followed

by flotation. The results in Figure 2 are expressed as the percentage of beads recovered in the froth as a function of the coverage of nanoparticles actually on the beads (i.e., the total projected area of nanoparticles/total area of bead surface). Note that the maximum coverage of randomly deposited noninteracting but nonoverlapping spheres is ~0.55, whereas electrostatic repulsion, tending to keep the spheres apart, gives an even lower maximum coverage.[20,21] The smaller, pure polystyrene nanoparticles, St-01-46, induced much greater glass bead removal than the larger nanoparticles bearing quaternary ammonium groups. Indeed, good bead recovery was observed with less than 10% of glass surface covered with smaller beads. This is an important observation because it suggests relatively low nanoparticle dosages could give good flotation. Since the early work of Gaudin and others, it has been known that less than 20% of a monolayer coverage of conventional surfactant collectors also can give good flotation (see Figure 4 in Fuerstenau's book[1]) Furthermore, surfactant collectors at low coverage are not uniformly distributed on the mineral surface. Instead, they are present as hemimicelles on the mineral surface.[22]

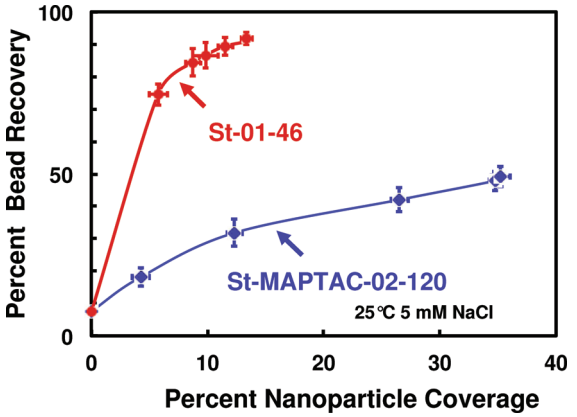

Figure 2. Influence of the density of adsorbed nanoparticles on glass bead (43 μm) recovery. Only one dish was collected.

The easy visualization of nanoparticles on mineral surfaces by electron microscopy is one of the advantages of nanoparticle flotation collectors. Figure 3 shows example scanning electron microscopy (SEM) micrographs of glass bead surfaces after flotation with three nanoparticle collectors. All micrographs show high coverages with no large bare patches. Closer examination reveals that the large St-MAPTAC-02-120 particles were mainly present as small aggregates, whereas the smaller St-01-46 was present mainly as individual particles. These observations underscore one of the challenges in the design of nanoparticle collectors. On one hand, a hydrophobic surface such as pristine polystyrene will favor flotation; on the other hand, hydrophilic ionic groups are required for nanoparticle colloidal stability.

Attachment of minerals to air bubbles is a fundamental requirement of flotation. Therefore, a necessary condition for flotation is a finite receding contact angle for the flotation medium on the mineral surface. In order to assess the ability of the nanoparticles to increase the contact angle, we conducted model experiments in which the cationic nanoparticles were

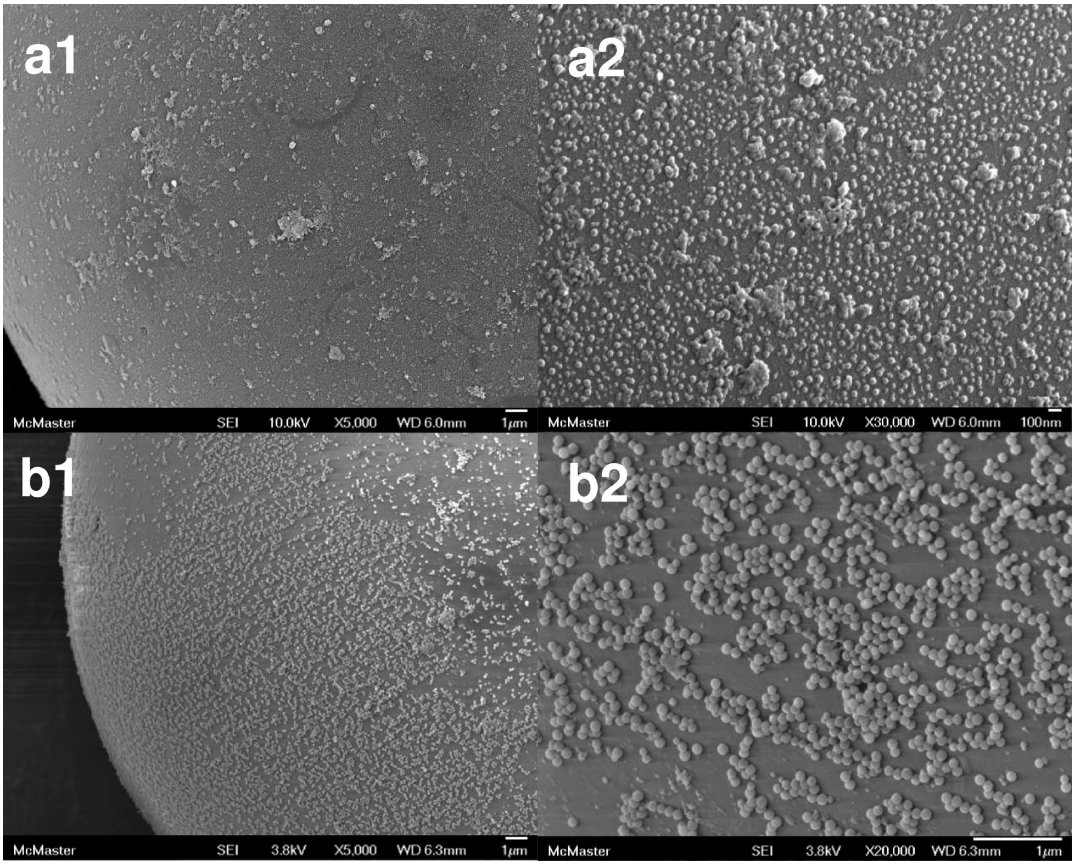

Figure 3. SEM images of dried 43 μm glass beads collected after flotation runs using 46 nm St-01-46 (a1,a2) and 120 nm St-MAPTAC-02-120 (b1,b2) nanoparticles.

dx.doi.org/10.1021/la2016534 |*Langmuir* 2011, 27, 10438–10446

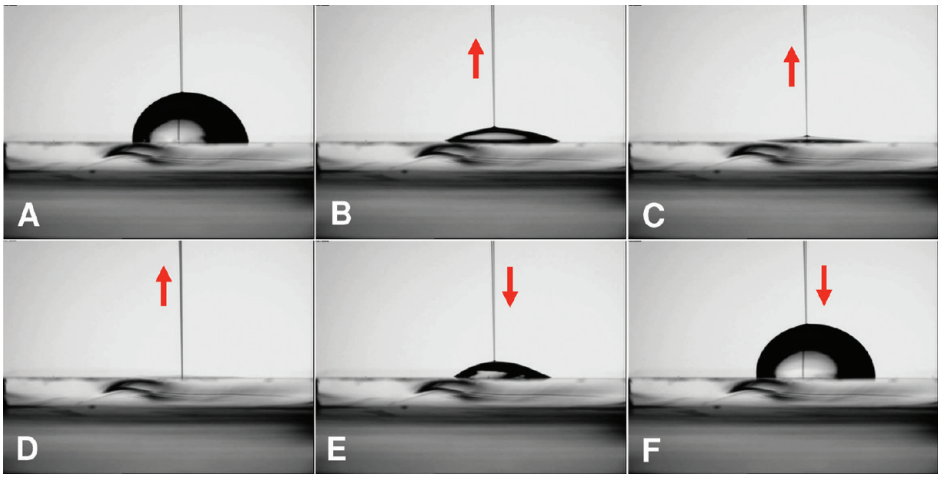

Figure 4. Decreasing and then increasing the volume of a sessile drop on glass decorated with deposited St-01-46 nanoparticles. The reappearance of the drop on the original footprint suggests that the receding contact line leaves wet patches on the surface.

allowed to deposit onto clean microscope slides on which we could easily measure water contact angles. In our initial experiments, we dried the glass slides decorated with nanoparticles and measured the advancing and receding water contact angle. Figure 4 shows images of the sessile drop in the sequence in which the drop was evacuated from the surface with a capillary tube and then pumped back onto the slide. The initial advancing angle was about 90°. When the liquid was withdrawn, the three-phase contact line was strongly pinned. Reversing the process, the drop reappeared on its original footprint, suggesting that the receding drop left water on the slide between the nanoparticles (wet patches on the glass).

Initially, we were concerned that the three-phase contact line (TPCL) pushed the glass beads on the glass slide, leaving a hydrophilic circle corresponding to the first drop. To prove that weak nanoparticle adhesion was not a problem, we repeated experiments on the same position on a slide after drying between measurements. The high advancing contact angle on the repeated experiment confirmed that the surface was not swiped clean in the first experiment. Other evidence of strong nanoparticle/glass adhesion includes the following: we took a sample of beads recovered from a flotation experiment and successfully refloated them without adding extra nanoparticles, and none of the electron micrographs of beads showed bare patches corresponding to nanoparticles being dragged on the bead surface.

In our flotation studies, the nanoparticles deposited onto glass bead surfaces submerged in water, with no drying step before bubble attachment. Therefore, we conducted contact angle measurements on immersed, never-dried surfaces, by introducing air bubbles from a micropipet and touching the bubbles to a modified glass surface. Figure 5 shows images of air bubbles on the surfaces of submerged glass slides. For images (a) and (b), glass slides spin coated with a solution formed by dissolving nanoparticle St-01-46 in THF were used. These surfaces were used to obtain an estimate of the equilibrium contact angle for the nanoparticle surfaces. The contact angles formed after bubble attachment were receding angles. Advancing angles were observed by using the micropipet to push the bubble across the surface. The advancing angle on spin coated polystyrene was θ_a = 93° ± 0.8°, whereas the receding angle of θ_r = 87° ± 1.6° was only slightly less.

Images (c) and (d) in Figure 5 show air bubbles on a glass surface decorated with St-01-46 nanoparticles. The advancing contact angle was θ_a = 61° ± 1.1°, whereas the more relevant receding angle was only θ_r = 17° ± 1.5°. Table 1 summarizes the key contact angle results for the two nanoparticles. With a cast film contact angle (θ_{np}) of 85°, St-MAPTAC-01-120 was only slightly less hydrophobic than St-01-46 with a contact angle of 91°. However, glass surfaces with a saturated layer of adsorbed particles, St-01-46 gave a contact angle (θ) of 40°, whereas the surface treated with St-MAPTAC-02-120 had an angle of only 23°. Thus, the larger nanoparticles, perhaps because of aggregation, were less effective in increasing contact angle.

All the contact angle measurements were made with pure water, whereas our flotation measurements were made with a frother solution of 5×10^{-3} M NaCl and 10 mg/L frother, a nonionic surfactant. The advancing water contact angle of the St-01-46 smooth polymer film decreased from 93° for water to 85° with frother solution, and the attached bubble receding contact angle decreased from 91° in water to 78° in the frother solution. Also, the surface tension of water decreased by about 3 mN/m with frother addition. Frothers are designed to enhance froth stability while having minimum negative impact on the ability of collectors to increase mineral hydrophobicity. This seems to be the case herein.

The attachment and detachment of nanoparticle-coated mineral were further characterized by the micromechanical measurement of adhesion forces holding a glass sphere to an air bubble. Suction was used to attach individual glass spheres to a micropipet that had been bent to give two 90° bends (right-angled Z-shaped) to serve as a cantilever. An air bubble attached to a second, larger pipet was pushed into the glass bead and then retracted. The forces were measured by the displacement of the calibrated cantilever. Details of our method have been published.[2,3] Figure 6 shows images from a measurement for a 55 μm diameter glass bead with deposited St-01-46 nanoparticles interacting with a 612 μm diameter air bubble. The plot shows measured force as a function of run time of the stepper motor that drives the capillary supporting the air bubble. For the first 10 s, the bubble was pushed against the glass bead, after which the direction was reversed and the force increased linearly with displacement until the bead detached from the bubble. The corresponding maximum pull-off force was 1.9 μN. We will show in the Discussion section that this value is consistent with

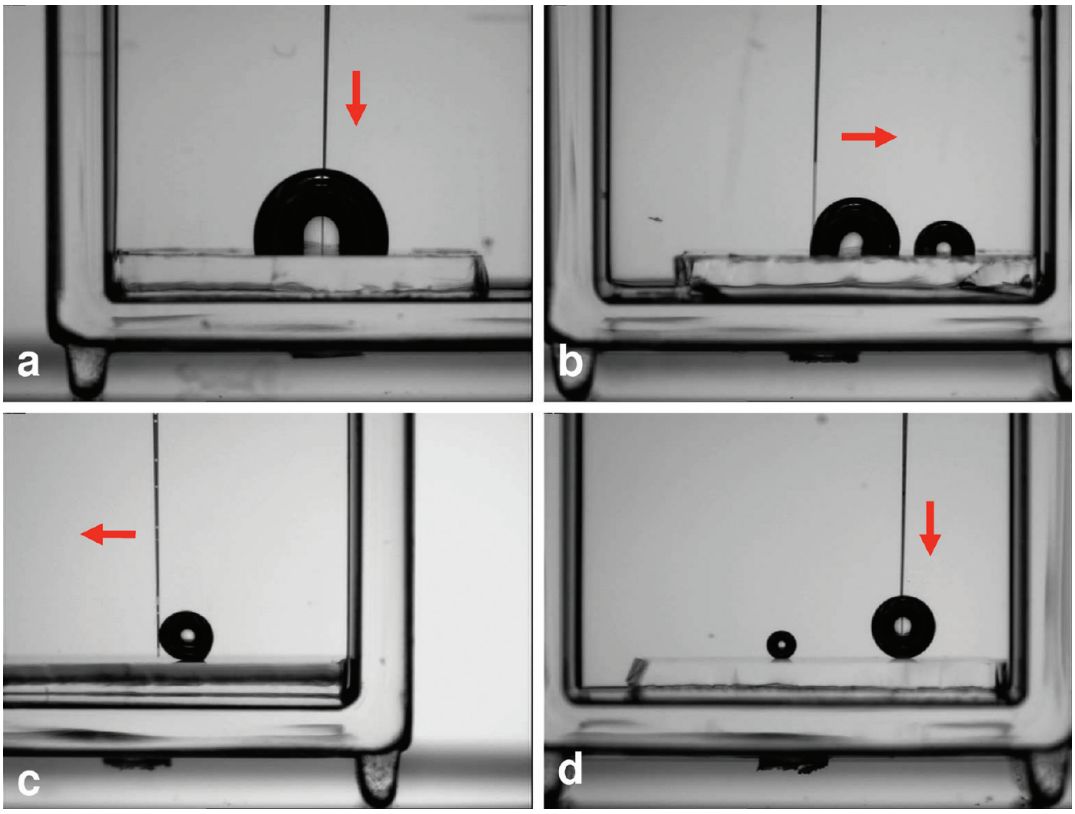

Figure 5. Submerged bubble-captive contact angle images. Frames (a) and (b) show smooth films prepared by spin coating with St-01-46 solution in THF. The corresponding contact angles are $\theta_a = 93° \pm 0.8°$, $\theta_r = 87° \pm 1.6°$, $\theta_s = 91° \pm 0.9°$, where subscripts denote a, advancing; b, receding; and s, static, the initial angle upon bubble adhesion. In frame (b), the capillary tubing was the left-hand pushing bubble. Frames (c) and (d) show never-dried glass surfaces with adsorbed St-01-46 nanoparticles giving contact angles of $\theta_a = 61° \pm 1.1°$, $\theta_r = 17° \pm 1.5°$, and $\theta_s = 40° \pm 1.6°$. In frame (c), the bubble was dragged by the capillary tube to generate receding and advancing angles.

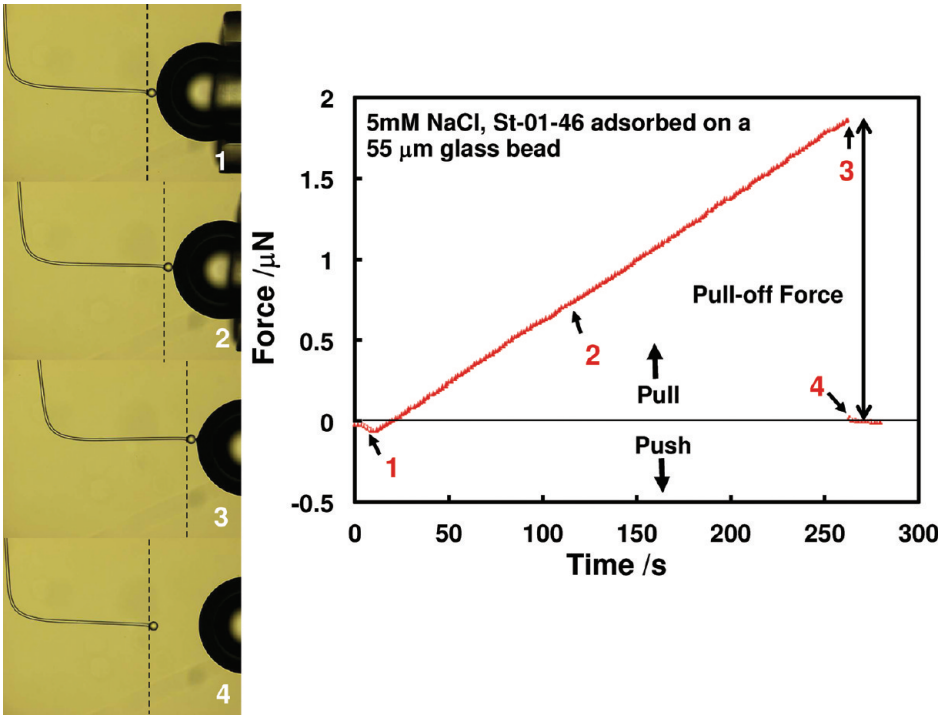

Figure 6. Example of a force versus displacement curve for attaching and removing a glass bead from an air bubble. Note that the displacement is expressed as the run time of the stepper motor driving the capillary supporting the air bubble. The bead diameter of 55 μm was measured from the image.

dx.doi.org/10.1021/la2016534 |*Langmuir* 2011, 27, 10438–10446

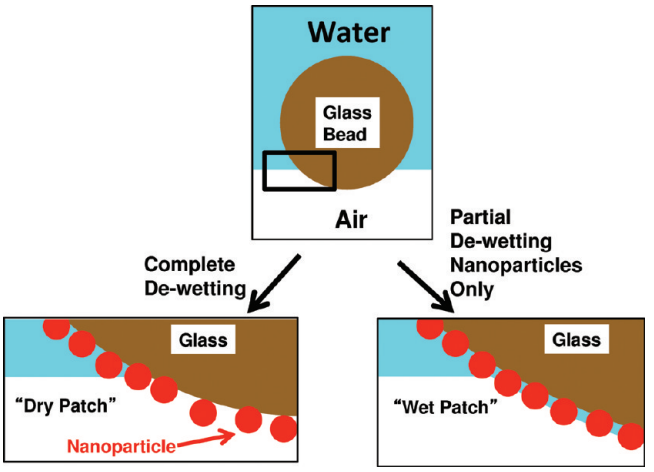

Figure 7. Three-phase contact point for two extreme cases of a bubble adhering to a glass sphere with adsorbed nanoparticles. Dry patch is the conventional case, whereas with the wet patch the three-phase contact lines are only on the nanoparticles.

theoretical predictions. Furthermore, there was no evidence of visible air pockets on the spheres after detachment. Measurements performed with clean, untreated beads yielded maximum pull-off forces of only 0.0086 μN.

DISCUSSION

There are a few obvious design parameters for nanoparticle flotation collectors, including nanoparticle shape, diameter, surface energy, and coverage on the mineral surface. The obvious role of nanoparticles is to facilitate mineral-bubble attachment and/or to minimize detachment. The goal of the following analysis is to consider the influence of nanoparticle parameters on the various stages of mineral particle flotation with a view to identifying the critical role of nanoparticles and to optimize nanoparticle properties. Specifically, the following analysis will try to explain the key behaviors shown in Figure 2; smaller, more hydrophobic particles are more efficient, and as little as 10% nanoparticle coverage gives high flotation yields.

The micromechanics experiments show a clear contact patch between the sphere and the bubble, approximately 10 μm in diameter. However, we do not know the detailed structure of this patch. At one extreme, the patch area could be completely dry, as we might expect from a receding three-phase contact line on a smooth hydrophobic surface. At the other extreme, we envision a bonding patch consisting of individual nanoparticles penetrating the air water interface, giving a bubble adhering with many isolated contacts to nanoparticles. The sessile drop experiment in Figure 4 suggests wet patch formation. We will now consider the potential role of nanoparticles in these two extreme cases: the conventional "dry patch" and the "wet patch" with nanoparticle contacts. Figure 7 schematically illustrates a conventional "dry patch" and a "wet patch". Since glass has a finite contact angle, we would expect that the actual situation is between the extremes, islands of water interspersed with the nanoparticles on the contact patch.

a. "Dry Patch" Adhesion. The collision of a bubble with a mineral particle causes the deformation of the bubble against the mineral particle surface, giving a thin aqueous film between the particle and the air. This transient structure can undergo two

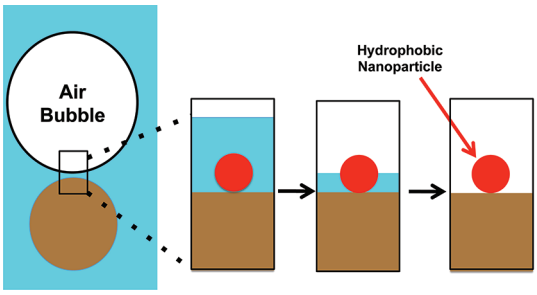

Figure 8. Thinning and rupture of the liquid film between a mineral particle with adsorbed nanoparticles and an air bubble.

fates. Either the bubble/mineral pair dissociates, or the liquid film thins and ruptures, resulting in mineral/bubble attachment. For mineral particle attachment to a bubble, Ralston et al. argue that the attachment step involves three processes: (1) thinning of the intervening liquid film between the mineral particle and the bubble; (2) rupture of the film to give a three-phase contact "nucleus"; and (3) expansion of the TPCL from the critical radius to form a stable wetting perimeter.[4]

The influence of small hydrophobic particles on the stability of thin liquid films has been extensively reported in the defoamer literature.[23,24] Defoamers employ small hydrophobic particles to nucleate the rupture of liquid films (lamella) between air bubbles. The relevant conclusions from defoamer studies are that hydrophobic particles do indeed nucleate film rupture; rough particles are more effective than smooth ones; and wax crystals and silicone coated silica particles a few micrometers in diameter are the most effective. By analogy with the defoamer particle mechanisms, we propose that one role for the nanoparticle collectors is to facilitate attachment by increasing the rupture thickness of the water film. In other words, less film drainage is required before rupture, thus increasing the probability of rupture. This mechanism is illustrated in Figure 8 showing that the nanoparticle serves as the dewetting "nucleus". We do not think that thinning and nucleus formation are rate determining because smaller particles are more effective; the minimum nanoparticle coverage is far greater than the very low coverage of particle required for nucleation; and our very limited data suggest that individual spheres are more effective at promoting flotation than are small nanoparticle aggregates.

Ralston's final step in the mineral/bubble attachment process is the expansion of the "contact nucleus" to a macroscopic contact area.[4] This is an expansion of the TPCL on a relatively hydrophilic surface with hydrophobic nanoparticle inclusions. The inverse of this problem (i.e., hydrophilic inclusions on a hydrophobic surface) has been discussed by de Gennes et al.[11] During the dewetting process, the TPCL must jump from hydrophobic patch to patch. The relevant distance scale is the minimum distance between neighboring nanoparticle surfaces. For the case of a square array of spheres on a plane, the minimum surface-to-surface distance between neighboring spheres, d_{ss}, is given by the following expression. The interparticle distance is linear with nanoparticle radius at constant coverage where r is the nanoparticle radius and λ is the coverage.

$$d_{ss} = r\left(\sqrt{\frac{\pi}{\lambda}} - 2\right) \quad (1)$$

In the absence of a specific model for the probability that the TPCL will expand, it seems reasonable to assume that the smaller

the value of d_{ss}, the more likely the initial contact nucleus will expand. Therefore eq 1 suggests that TPCL expansion is promoted by increasing the nanoparticle coverage, λ, and by decreasing the nanoparticle radius. Both of these predictions are in accord with the experimental results in Figure 2.

We now discuss the influence nanoparticle size, hydrophobicity, and coverage on the maximum force required to pull a glass bead from an equilibrium position on the air/water interface into the aqueous phase. Scheludko et al. derived the following expression where R_m is the radius of the glass sphere, γ is the surface tension, and θ is the contact angle.[25,26]

$$F_{dry} = 2\pi R_m \gamma \sin\left(\pi - \frac{\theta}{2}\right) \sin\left(\pi + \frac{\theta}{2}\right) = 2\pi R_m \gamma \sin^2\left(\frac{\theta}{2}\right) \quad (2)$$

b. "Wet Patch" Adhesion. Our vision of the structure of a wet patch (see Figure 7) is essentially the same as that proposed by Takeshita et al. for the structure of water sitting on a dense layer of latex deposited on a film.[15] The radius of the wet patch, R_w, can be expressed as the following function of the apparent contact angle, θ, formed between the bubbles and mineral. In our work, θ was estimated from contact angles of bubbles adhering to immersed flat surfaces (see Figure 5 and Table 1).

$$R_w = R_m \sin(\theta) \quad (3)$$

We assume that the maximum pull-off force from a wet patch is determined by the nanoparticles on the wet patch periphery. In other words, bead/bubble separation is essentially peeling, and the maximum peel force corresponds to the maximum perimeter of the contact patch. The following expression comes directly where ζ is the number of nanoparticles per length of line defining the outer edge of the contact patch and θ_{np} is the contact angle of the nanoparticle surface. Note we measured θ_{np} by casting the particles into smooth thin films and the values were about 90° (see Figure 5a and b for examples).

$$F_{wet} = 2\pi R_w \zeta 2\pi r\gamma \sin^2\left(\frac{\theta_{np}}{2}\right) \quad (4)$$

If the nanoparticles are randomly distributed, including allowing overlapping particles, ζ is given by the following expression where N is the number of nanoparticles per unit area.

$$\zeta = N2r = \frac{\lambda}{\pi r^2} 2r = \frac{2\lambda}{\pi r} \quad (5)$$

Substituting eqs 3 and 5 into eq 4 gives the following expression for the maximum pull-off force from a wet patch.

$$F_{wet} = 8\pi R_m \sin(\theta)\lambda\gamma \sin^2\left(\frac{\theta_{np}}{2}\right) \quad (6)$$

The wet patch peel analysis, eq 6, predicts no dependence of pull-off force on nanoparticle size, whereas the nanoparticle coverage, λ, and nanoparticle hydrophobicity, θ_{np}, are important. To compare the dry patch (eq 2) and wet patch models (eq 6) to our experimental pull-off forces (Figure 6), values are required for λ and θ; neither was measured during the micromechanics experiment. The Cassie–Baxter contact angle model gives the following relationship between θ and λ where θ_m is the contact angle on the clean glass, which is about 5°.

$$\cos(\theta) = \lambda \cos(\theta_{np}) + (1 - \lambda) \cos(\theta_m) \quad (7)$$

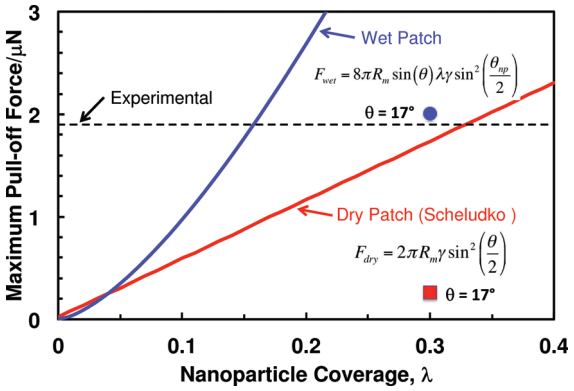

Figure 9. Comparing the predictions of the conventional dry patch theory (eq 2) and wet patch theory (eq 6) with the experimental result. The Cassie–Baxter equation (eq 7) was used to estimate the bubble/bead contact angle, θ, as a function of λ. The parameters used for the calculation were: R_m = 27.5 μm, θ_m = 5°, θ_{np} = 87°, and γ = 70 mN/m. For the two individual points, we used θ = 17° (from immersed bubble measurements, Figure 5) and λ = 30% (an estimate).

Figure 9 compares the maximum pull-off force as a function of nanoparticle coverage. For coverages above 5%, the wet patch analysis predicts higher pull-off forces than does the conventional dry patch analysis. Both models predict substantial adhesion forces at low coverages, confirming the experimental observation that 5–10% coverage can give high flotation recoveries (see Figure 2). However, we have serious concerns about estimating the contact angle with the Cassie–Baxter equation, which seems to overestimate the angles. For example, the micromechanics experiments were conducted under conditions which should nearly saturate the bead with adsorbed nanoparticles giving $\lambda \sim$ 30%. The corresponding value of θ, from eq 7 is 45°, which is high compared to the 17° we measured in our bubble attachment experiments. Substituting 45 in eq 3 gives a radius of the bead/bubble contact patch of 19 μm, whereas the micromechanics images suggest a contact radius of ~5 μm. Thus, the Cassie–Baxter analysis is overestimating the contact angles. Taking our experimental bubble attachment contact angle, θ = 17°, and estimating λ = 30% gives the two points plotted in Figure 9. The wet patch analysis gives a very good estimate of the experimental result.

Key parameters for both pull-off force models are the nanoparticle coverage and the hydrophobicity of the nanoparticles; neither model predicts that nanoparticle radius is important for pull-off force. Within the uncertainty of the parameters, particularly the radius of the contact patch (R_w), we cannot reject either of the models (i.e., eq 2 or 6). Further experiments are required to fully understand the nature of the contact zone between an air bubble and a hydrophilic surface coated with hydrophobic nanoparticles.

In summary, the air bubble attachment experiments, Figure 5, and the micromechanics experiments demonstrate that nanoparticles promote bubble attachment and give large pull-off forces. Our analysis predicts that both attachment and pull-off forces increase with increasing coverage, λ, and decreasing nanoparticle contact angle (θ_{np}). Furthermore, the initial bubble attachment should be facilitated by larger nanoparticles that will

nucleate the rupture of the aqueous film between the bubble and the mineral.

CONCLUSIONS

This work is the first report of a novel application for nanoparticles as flotation collectors. From a scientific perspective, there are many unanswered questions about the detailed role of the nanoparticles. From a technological perspective, a critical issue is the ability to selectively deposit the nanoparticles onto surfaces of the desired mineral particles in a complex mixture. A future publication will show that nanoparticles can be designed to selectively deposit onto a nickel mineral (pentlandite) in the presence of gangue. The main conclusions from the current work are as follows:

1. Nanoparticles based on polystyrene function as flotation collectors if they adsorb onto mineral surfaces.
2. High flotation efficiencies can be achieved with less than 10% coverage of the glass beads, a mineral model.
3. Smaller and more hydrophobic nanoparticles are the most efficient flotation collectors.
4. The forces required to pull a nanoparticle-coated sphere from the air/water interface of a bubble into the water was determined via micromechanical measurements. The maximum pull-off force ranged from 0.0086 μN for a clean 55 μm glass bead to 1.9 μN for a bead bearing adsorbed 46 nm diameter polystyrene spheres.
5. We propose that the patch where a glass sphere intersects the bubble could be wet, except where nanoparticles protrude through the air/water interface, that is, a wet patch. The pull-off force for a wet patch can be estimated by a peel analysis where the exterior ring of particles on the wet patch accounts for the adhesion. Clearly, more work is required to verify the wet patch hypothesis.

AUTHOR INFORMATION

Corresponding Author

*E-mail: peltonrh@mcmaster.ca.

ACKNOWLEDGMENT

We thank the Centre for Materials and Manufacturing (CMM), a division of the Ontario Centres of Excellence (OCE) in collaboration with VALE Base Metals for funding; VALE, Base Metals Technology Development for funding; and Zongfu Dai and Manqiu Xu from Vale for much help, samples, and advice. Finally, we acknowledge Prof. Ramin Farnood, University of Toronto, and Prof. Lee White, University of South Australia, for mechanistic discussions.

REFERENCES

(1) *Froth Flotation: A Century of Innovation*; Fuerstenau, M., Jameson, G., Yoon, R., Eds.; Society for Mining, Metallurgy, and Exploration: Littleton, CO, 2007.

(2) Yeung, A. K. C.; Pelton, R.; Micromechanics, A New Approach to Studying the Strength and Breakup of Flocs. *J. Colloid Interface Sci.* **1996**, *184*, 579–585.

(3) Colbert, M. J.; Raegen, A. N.; Fradin, C.; Dalnoki-Veress, K. Adhesion and Membrane Tension of Single Vesicles and Living Cells Using a Micropipette-Based Technique. *Eur. Phys. J. E* **2009**, *30*, 117–121.

(4) Nguyen, A. V.; Schulze, H. J.; Ralston, J. Elementary Steps in Particle--Bubble Attachment. *Int. J. Miner. Process.* **1997**, *51*, 183–195.

(5) Wark, I. W. The Physical Chemistry of Flotation. I. The Significance of Contact Angle in Flotation. *J. Phys. Chem.* **1933**, *37*, 623–644.

(6) Gontijo, C. D.; Fornasiero, D.; Ralston, J. The Limits of Fine and Coarse Particle Flotation. *Can. J. Chem. Eng.* **2007**, *85*, 739–747.

(7) Pyke, B.; Fornasiero, D.; Ralston, J. Bubble Particle Heterocoagulation under Turbulent Conditions. *J. Colloid Interface Sci.* **2003**, *265*, 141–151.

(8) Chau, T. T.; Bruckard, W. J.; Koh, P. T. L.; Nguyen, A. V. A Review of Factors That Affect Contact Angle and Implications for Flotation Practice. *Adv. Colloid Interface Sci.* **2009**, *150*, 106–115.

(9) Pitois, O.; Chateau, X. Small Particle at a Fluid Interface: Effect of Contact Angle Hysteresis on Force and Work of Detachment. *Langmuir* **2002**, *18*, 9751–9756.

(10) Gillies, G.; Kappl, M.; Butt, H. J. Direct Measurements of Particle-Bubble Interactions. *Adv. Colloid Interface Sci.* **2005**, *114*, 165–172.

(11) De Gennes, P. G.; Brochard-Wyart, F.; Quèrè, D. *Capillarity and Wetting Phenomena: Drops, Bubbles, Pearls, Waves*; Springer Verlag: New York, 2004.

(12) Priest, C.; Sedev, R.; Ralston, J. Asymmetric Wetting Hysteresis on Chemical Defects. *Phys. Rev. Lett.* **2007**, *99*, 026103.

(13) Yan, L.; Wang, K.; Wu, J.; Ye, L. Hydrophobicity of Model Surfaces with Closely Packed Nano- and Micro-Spheres. *Colloids Surf., A* **2007**, *296*, 123–131.

(14) Yan, L.; Wang, K.; Wu, J.; Ye, L. Hydrophobicity of Model Surfaces with Loosely Packed Polystyrene Spheres after Plasma Etching. *J. Phys. Chem. B* **2006**, *110*, 11241–11246.

(15) Takeshita, N.; Paradis, L. A.; Öner, D.; Mccarthy, T. J.; Chen, W. Simultaneous Tailoring of Surface Topography and Chemical Structure for Controlled Wettability. *Langmuir* **2004**, *20*, 8131–8136.

(16) Watanabe, M.; Kawaguchi, S.; Nagai, K. Self-Organization of Polymer Particles on Hydrophobic Solid Substrates in Aqueous Media. Ii. Self-Organization of Cationic Polymer Particles on Polymer Films and Wettability Control with Particle Monolayers. *Colloid Polym. Sci.* **2007**, *285*, 1139–1147.

(17) Fetzer, R.; Ralston, J. Dynamic Dewetting Regimes Explored. *J. Phys. Chem. C* **2009**, *113*, 8888–8894.

(18) Goodwin, J. W.; Ottewill, R. H.; Pelton, R. Studies on the Preparation and Characterization of Monodisperse Polystyrene Lattices. 5. Preparation of Cationic Lattices. *Colloid Polym. Sci.* **1979**, *257*, 61–69.

(19) Sajjadi, S. Nanoparticle Formation by Monomer-Starved Semi-batch Emulsion Polymerization. *Langmuir* **2006**, *23*, 1018–1024.

(20) Adamczyk, Z.; Dabros, T.; Czarnecki, J.; Vandeven, T. G. M. Particle Transfer to Solid-Surfaces. *Adv. Colloid Interface Sci.* **1983**, *19*, 183–252.

(21) Adamczyk, Z.; Zembala, M.; Siwek, B.; Warszynski, P. Structure and Ordering in Localized Adsorption of Particles. *J. Colloid Interface Sci.* **1990**, *140*, 123–137.

(22) Atkin, R.; Craig, V. S. J.; Wanless, E. J.; Biggs, S. Mechanism of Cationic Surfactant Adsorption at the Solid-Aqueous Interface. *Adv. Colloid Interface Sci.* **2003**, *103*, 219–304.

(23) Garrett, P. *Defoaming: Theory and Industrial Applications*; CRC Press: Boca Raton, FL, 1993.

(24) Wang, G.; Pelton, R.; Hrymak, A.; Shawafaty, N.; Heng, Y. M. On the Role of Hydrophobic Particles and Surfactants in Defoaming. *Langmuir* **1999**, *15*, 2202–2208.

(25) Scheludko, A.; Toshev, B. V.; Bojadjiev, D. T. Attachment of Particles to a Liquid Surface (Capillary Theory of Flotation). *J. Chem. Soc., Faraday Trans. 1* **1976**, *72*, 2815–2828.

(26) Fielden, M. L.; Hayes, R. A.; Ralston, J. Surface and Capillary Forces Affecting Air Bubble−Particle Interactions in Aqueous Electrolyte. *Langmuir* **1996**, *12*, 3721–3727.